The endocannabinoid *N*-arachidonoyl glycine (NAGly) inhibits store-operated Ca^{2+} entry by preventing STIM1–Orai1 interaction

Andras T. Deak, Lukas N. Groschner, Muhammad Rizwan Alam, Elisabeth Seles, Alexander I. Bondarenko, Wolfgang F. Graier and Roland Malli*

Institute of Molecular Biology and Biochemistry, Center of Molecular Medicine, Medical University Graz, Graz, Austria

*Author for correspondence (roland.malli@medunigraz.at)

Accepted 16 November 2012
Journal of Cell Science 126, 879–888

doi: 10.1242/jcs.118075

Summary

The endocannabiniod anandamide (AEA) and its derivate *N*-arachidonoyl glycine (NAGly) have a broad spectrum of physiological effects, which are induced by both binding to receptors and receptor-independent modulations of ion channels and transporters. The impact of AEA and NAGly on store-operated Ca^{2+} entry (SOCE), a ubiquitous Ca^{2+} entry pathway regulating many cellular functions, is unknown. Here we show that NAGly, but not AEA reversibly hinders SOCE in a time- and concentration-dependent manner. The inhibitory effect of NAGly on SOCE was found in the human endothelial cell line EA.hy926, the rat pancreatic β-cell line INS-1 832/13, and the rat basophilic leukemia cell line RBL-2H3. NAGly diminished SOCE independently from the mode of Ca^{2+} depletion of the endoplasmic reticulum, whereas it had no effect on Ca^{2+} entry through L-type voltage-gated Ca^{2+} channels. Enhanced Ca^{2+} entry was effectively hampered by NAGly in cells overexpressing the key molecular constituents of SOCE, stromal interacting molecule 1 (STIM1) and the pore-forming subunit of SOCE channels, Orai1. Fluorescence microscopy revealed that NAGly did not affect STIM1 oligomerization, STIM1 clustering, or the colocalization of STIM1 with Orai1, which were induced by Ca^{2+} depletion of the endoplasmic reticulum. In contrast, independently from its slow depolarizing effect on mitochondria, NAGly instantly and strongly diminished the interaction of STIM1 with Orai1, indicating that NAGly inhibits SOCE primarily by uncoupling STIM1 from Orai1. In summary, our findings revealed the STIM1–Orai1-mediated SOCE machinery as a molecular target of NAGly, which might have many implications in cell physiology.

Key words: Anandamide, Calcium imaging, Endocannabinoids, Endothelial cells, Fluorescent proteins, Fluorescence microscopy, FRET, Fura-2, INS-1 cells, NAGly

Introduction

Endocannabinoids are signaling lipids that modulate a multitude of physiological functions. Initially, *N*-arachidonoylethanolamid, also referred to as anandamide (AEA), and 2-aracidonoylglycerol (2-AG) were identified as natural ligands of the cannabinoid receptors CB_1 and CB_2 and their psychoactive effects in the central nervous system (CNS) were established (Pertwee, 2006; Mechoulam, 2002). However, evidence accumulated recently that the actions of these endocannabinoids and many other structurally related compounds are not restricted to the CNS. In particular, endocannabinoids have been implicated in the regulation of the immune system (Tanasescu and Constantinescu, 2010), the gastrointestinal tract (Izzo et al., 2001), and the cardiovascular system (Kunos et al., 2002). Interestingly, the broad spectrum of physiological functions modulated by endocannabinoids is only partially based on their binding to the classical cannabinoid receptors CB_1 and CB_2. Additional receptors such as the 'orphan' G-protein-coupled receptors GPR18 (Kohno et al., 2006) and GPR55 (Waldeck-Weiermair et al., 2008) have also been identified as targets of endocannabinoids. Moreover, recent studies indicate that endocannabinoids directly modulate the activity of diverse ion channels. Effects that are, at least in part, independent from G-protein-coupled receptors include the modulation of Ca^{2+}-activated K^+ channels (Parmar and Ho, 2010; Bondarenko et al., 2011a), the inhibition of voltage-gated Ca^{2+} channels (Barbara et al., 2009), and the activation of non-selective cation channels (Zygmunt et al., 1999). These receptor-independent actions of endocannabinoids have been described in human endothelial cells (Waldeck-Weiermair et al., 2008; Bondarenko et al., 2011b) and point to the capability of these lipid mediators to modulate the cellular ion homeostasis of non-excitable cells.

In this particular cell type, the major Ca^{2+} entry pathway is the so-called store-operated Ca^{2+} entry (SOCE) (Parekh and Putney, 2005). The activation of SOCE is triggered by Ca^{2+} depletion of the endoplasmic reticulum (ER), whereupon the decrease of the ER Ca^{2+} concentration ($[Ca^{2+}]_{ER}$) is sensed by the stromal interacting molecule 1 (STIM1) (Roos et al., 2005; Liou et al.,

Journal of Cell Science

2005), which oligomerizes and redistributes to subplasmalemmal ER domains, forming so-called STIM1 clusters (Wu et al., 2006; Luik et al., 2008; Liou et al., 2007). Subsequently, the interaction of STIM1 with the SOCE pore-forming subunit Orai1 (Vig et al., 2006; Park et al., 2009; Yuan et al., 2009) enables robust Ca^{2+} influx.

Although the molecular mechanisms of SOCE activation and the contributing proteins are well described (Liou et al., 2005; Roos et al., 2005; Mercer et al., 2006; Feske et al., 2006), little is known about regulatory mechanisms that modulate this important Ca^{2+} entry pathway. In view of the recent findings regarding endocannabinoids as modulators of the cellular ion homeostasis,

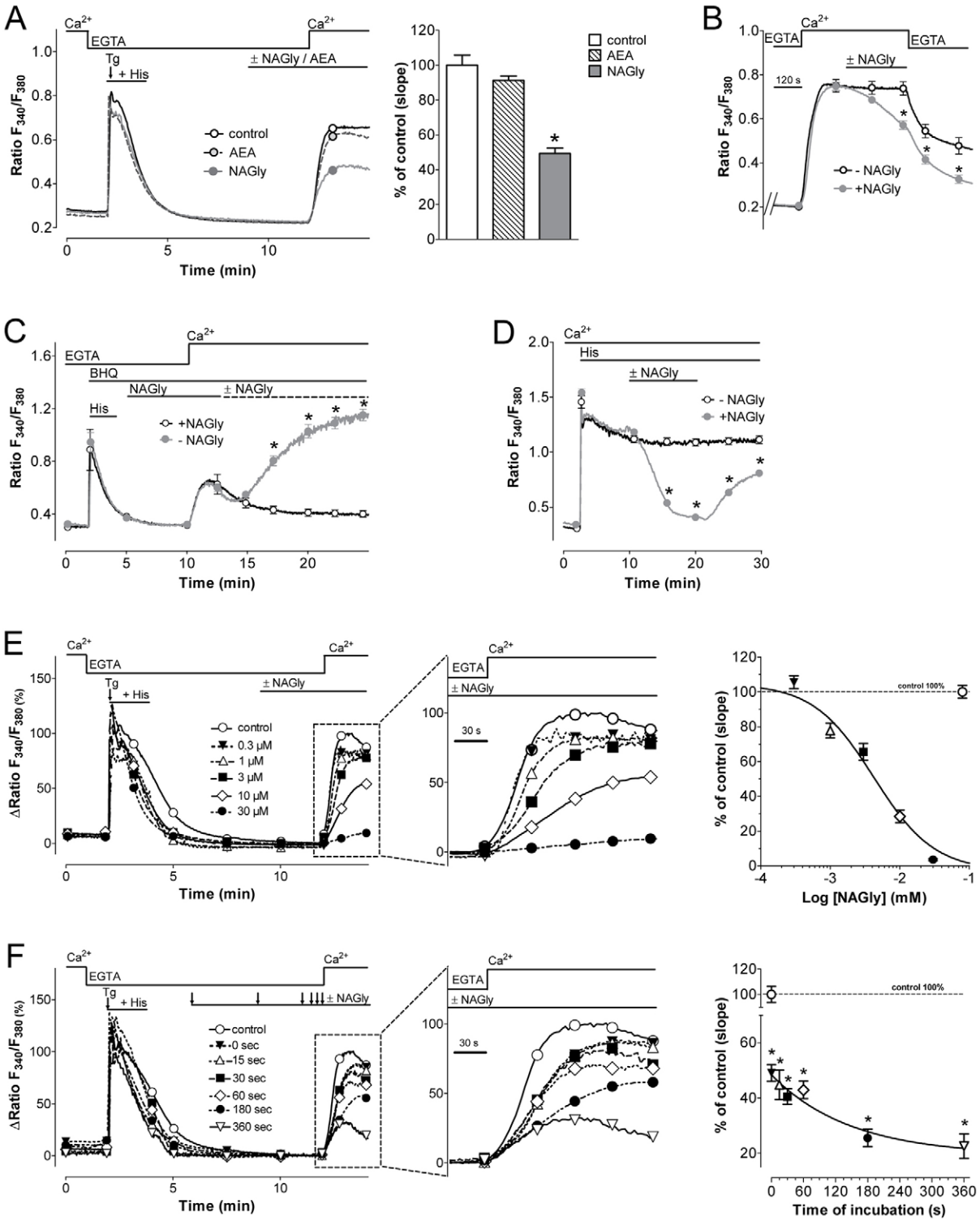

Fig. 1. See next page for legend.

this study was designed to elucidate the potential contribution of endocannabinoids to SOCE. For this purpose, AEA and its derivate *N*-arachidonoyl glycine (NAGly) (Bradshaw et al., 2009) which, in contrast to AEA, has no affinity to bind to CB_1 and CB_2 (Sheskin et al., 1997), were tested on SOCE activity. Our experiments revealed that NAGly, but not AEA, impairs the interaction of STIM1 with Orai1 and is highly effective in inhibiting SOCE, thus, demonstrating for the first time that the STIM1–Orai1-mediated SOCE machinery represents a specific target of an endocannabinoid. Although the metabolic origin of NAGly is not completely resolved, the wide distribution of this mediator in mammalian tissues (Huang et al., 2001) supports the notion that the inhibitory effect of NAGly on SOCE shown herein may also essentially contribute to the regulation of many physiological functions *in vivo*.

Results and Discussion

NAGly but not AEA reversibly inhibits SOCE activity in a concentration- and time-dependent manner

The effects of AEA and its derivate NAGly on SOCE signals in single cells of the human umbilical vein-derived endothelial cell line EA.hy926 were tested. Therefore, the classical Ca^{2+} re-addition protocol (Putney, 1986) was performed by stimulating fura-2/AM loaded cells with thapsigargin (Tg) and histamine in the absence of extracellular Ca^{2+} followed by addition of extracellular Ca^{2+} in the presence of the compound to be tested. While 10 µM AEA did not affect SOCE, it was significantly diminished in the presence of 10 µM NAGly (Fig. 1A), thus, indicating that the two structurally related endocannabinoids clearly differ in terms of their potency to impact SOCE in endothelial cells. Control experiments without cell stimulation ruled out the occurrence of Ca^{2+} entry without ER Ca^{2+} depletion in these cells (supplementary material Fig. S1A). In line with previous reports (Kohno et al., 2006), NAGly slowly mobilized Ca^{2+} from the ER in the absence of Tg/His, however, SOCE was not activated (supplementary material Fig. S1A). Moreover, once the Ca^{2+} entry maximally developed and reached a plateau upon Ca^{2+} addition, NAGly was able to reduce $[Ca^{2+}]_{cyto}$ (Fig. 1B). The impairment of Ca^{2+} entry by NAGly persisted only as long as the compound was present (Fig. 1C), indicating that the inhibitory effect of NAGly on SOCE is reversible.

Next, we tested the effect of NAGly on SOCE signals in endothelial cells that were stimulated exclusively with the inositol 1,4,5-trisphosphate-generating agonist histamine (His). Under these conditions $[Ca^{2+}]_{cyto}$ rapidly increased and reached a stable plateau of elevated $[Ca^{2+}]_{cyto}$ (Fig. 1D) which was shown to depend on continuous Ca^{2+} influx (Malli et al., 2003). The addition of NAGly at the plateau strongly attenuated $[Ca^{2+}]_{cyto}$ which recovered following NAGly removal (Fig. 1D). These findings demonstrated that NAGly also reversibly inhibits Ca^{2+} entry if cells are exclusively stimulated with an inositol 1,4,5-trisphosphate-generating agonist.

It was previously suggested that under such conditions of cell stimulation a receptor-activated Ca^{2+} entry (RACE) (Jousset et al., 2008) is activated in EA.hy926 cells in addition to SOCE, which is independent from ER Ca^{2+} depletion. Therefore, we tested whether or not the inhibitory effect of NAGly on Ca^{2+} entry remains the same if ER Ca^{2+} stores are depleted with Tg alone. These experiments showed that NAGly reduced SOCE signals to the same extent independently from the mode of ER Ca^{2+} depletion (supplementary material Fig. S1B). Moreover, our results indicate that cell stimulation with His is not essential for the inhibitory effect of NAGly on Ca^{2+} entry, pointing to SOCE rather than RACE as a likely target of this endocannabinoid in endothelial cells.

The inhibitory effect of NAGly on cytosolic SOCE signals in endothelial cells showed a clear concentration–response relationship for both the slopes (Fig. 1E) and amplitudes (supplementary material Fig. S1C) of respective rises in $[Ca^{2+}]_{cyto}$ upon Ca^{2+} addition. Notably, the half maximal inhibitory concentration (IC_{50}) of NAGly to attenuate the slope of rises in $[Ca^{2+}]_{cyto}$ upon Ca^{2+} addition in endothelial cells was found to be 4.22 (1.82–9.87) µM.

Analogous experiments were performed in RBL-2H3 cells, a mast cell model, which exhibits robust Ca^{2+} entry via SOCE (Schindl et al., 2002). In line with our findings in endothelial cells, NAGly was similarly effective to inhibit SOCE-driven $[Ca^{2+}]_{cyto}$ rises in RBL-2H3 cells (supplementary material Fig. S1D). The IC_{50} of NAGly on SOCE perfectly matches the effective concentration of NAGly to reduce inflammatory processes (Burstein et al., 2011). Considering the fundamental role of SOCE in immune cells (Shaw and Feske, 2012), the inhibitory

Fig. 1. NAGly but not AEA inhibits SOCE signals in endothelial cells. (**A**) Left panel: representative curves of Fura-2/AM-loaded EA.hy926 cells stimulated for 2 minutes with 1 µM thapsigargin (Tg) and 100 µM histamine (His) in 1 mM EGTA. 3 minutes prior to Ca^{2+} addition cells were treated with either ethanol (control; black line, $n=60$ cells/6 independent experiments) or 10 µM NAGly (grey line, $n=81/6$) or 10 µM anandamide (AEA, dashed line, $n=77/6$) Right panel: bars represent mean slopes of Ca^{2+} increase upon Ca^{2+} re-addition, from the curves shown in the left panel. $^*P<0.0001$ versus control. (**B**) $[Ca^{2+}]_{cyto}$ elevation in response to Ca^{2+} addition after ER Ca^{2+} depletion as described in A. Once Ca^{2+} entry reached a steady state, cells were treated with 10 µM NAGly (grey, filled circles, 33/3) or left untreated (black, open circles $n=29/3$). $^*P<0.0001$ versus −NAGly. (**C**) Representative curves showing the effect of NAGly washout (−NAGly, grey, filled circles, $n=10$) during SOCE. In respective control experiments, NAGly was present until the end (+NAGly, black, open circles $n=25$). 15 µM BHQ was used for sarcoendoplasmic reticulum calcium transport ATPase inhibition. $^*P<0.0001$ versus +NAGly. (**D**) The reversibility of 10 µM NAGly on $[Ca^{2+}]_{cyto}$ elevation was tested during cell stimulation with 100 µM histamine in the presence of 2 mM Ca^{2+} (−NAGly, black, open circles $n=16$; +NAGly, grey, filled circles, $n=17$): $^*P<0.0001$ versus −NAGly. (**E**) Left panel; concentration–response experiments regarding the inhibitory effect of NAGly on SOCE in protocols as described in A. Cells were incubated with 0.3–30 µM concentrations of NAGly ($n=20$–30 cells each), while control cells ($n=34$) received no treatment. The F_{340}/F_{380} ratio was normalized to the maximal Ca^{2+} entry of control cells, where the delta maximum of $[Ca^{2+}]_{cyto}$ elevation in response to Ca^{2+} addition was defined as 100%. Middle panel: enlargement of the Ca^{2+} entry phases displayed in the left panel. Right panel: concentration–inhibition curve of NAGly on SOCE. Symbols indicate the slopes of $[Ca^{2+}]_{cyto}$ elevation upon Ca^{2+} addition as a percentage of control. Data were fitted with a dose–inhibition sigmoidal equation. $IC_{50}=4.22$ (1.82–9.87) µM. (**F**) Left panel: the time-dependent effect of NAGly on SOCE. After ER Ca^{2+} depletion cells were incubated with 10 µM NAGly starting 360, 180, 60, 30 or 15 s prior to, or simultaneously with (0 s), Ca^{2+} addition as indicated by arrows ($n=13$–20 cells each). The F_{340}/F_{380} ratio was normalized to the maximal Ca^{2+} entry (considered as 100%) of control cells ($n=24$) which did not receive NAGly. Middle panel: enlargement of the Ca^{2+} entry phases displayed in the left panel. Right panel: incubation-time-dependent inhibitory effect of NAGly on SOCE. Symbols indicate the slopes of $[Ca^{2+}]_{cyto}$ elevation upon Ca^{2+} addition as a percentage of control. $^*P<0.0001$ versus control.

effect of NAGly on SOCE described herein may at least partially explain the immune-modulating actions of endocannabinoids. Moreover, SOCE is of utmost importance to stimulate the biosynthesis of multiple factors in endothelial cells (Graier et al., 1994), such as nitric oxide, prostaglandin (Lückhoff et al., 1988) and endothelin-1 (Brunner et al., 1994). Although a more detailed investigation is necessary, it is tempting to speculate that the effects of NAGly in the vasculature are, at least in part, due to its inhibitory potential on SOCE. Even though it has been estimated that the concentration of NAGly on potential sites of action vary between 5 and 24 μM (Wiles et al., 2006), the actual steady-state concentration of NAGly *in vivo* is not known, difficult to assess and depends on its rates of synthesis and hydrolysis. However, it is possible that local concentrations of lipid molecules, such as NAGly, might even exceed the μM range *in vivo* (Zaccagnino et al., 2009). Furthermore, we tested if a certain concentration of NAGly attenuates SOCE signals in a time-dependent manner. For this purpose, cells were pretreated with NAGly for different periods of time prior to Ca^{2+} addition after ER Ca^{2+} depletion. These experiments revealed that the magnitude of the inhibitory effect of NAGly on both the slopes (Fig. 1F) and amplitudes (Fig. 1F; supplementary material Fig. S1E) of SOCE correlated with the time period of preincubation. These findings indicate that NAGly might trigger a cellular signaling cascade in order to mediate the inhibitory effect on SOCE. Such an assumption is in line with a recent report demonstrating the activity of certain kinases, such as ERK1/2, to regulate SOCE activity (Pozo-Guisado et al., 2010). Since intact respiring mitochondria have been recognized to be fundamental for the activation, maintenance and termination of SOCE (Naghdi et al., 2010; Graier et al., 2007; Schwindling et al., 2010; Parekh, 2008), we tested the impact of NAGly on mitochondria in intact endothelial cells. In line with a previous study using isolated liver mitochondria (Zaccagnino et al., 2009), NAGly was indeed effective in acidifying and depolarizing mitochondria of endothelial cells (supplementary material Fig. S2), however, with a delay in time. Consequently, the temporal correlation (supplementary material Fig. S2) indicates that the NAGly-induced depolarization of mitochondria is not likely to be the cause of the instant repression of this Ca^{2+} entry pathway.

NAGly does not affect Ca^{2+} influx through voltage-gated Ca^{2+} channels but reduces the increase in SOCE signals in cells coexpressing STIM1 and Orai1

In order to verify whether the inhibitory effect of NAGly on SOCE is specific for this particular Ca^{2+} entry route, the impact of NAGly on Ca^{2+} influx through voltage-gated Ca^{2+} channels was tested using the pancreatic β-cell line INS-1 832/13 (INS-1). Like many other excitable cells, pancreatic β-cells are equipped with both L-type voltage-dependent Ca^{2+} channels (Nitert et al., 2008) and the SOCE machinery (Dyachok and Gylfe, 2001), which provides the possibility to test NAGly on these two distinct Ca^{2+} entry pathways in the same cell type. Treatment with 30 mM K^+ in the presence of 20 mM glucose (Dyachok and Gylfe, 2001) triggered Ca^{2+} entry exclusively via voltage-gated Ca^{2+} channels in INS-1 cells, resulting in a fast elevation of $[Ca^{2+}]_{cyto}$ that was insensitive to NAGly (Fig. 2A). This is in line with a previous study using HEK cells, in which NAGly failed to inhibit the L-type voltage-dependent Ca^{2+} channel (Barbara et al., 2009). In agreement with our findings in endothelial and mast cells described above, NAGly also significantly reduced Ca^{2+} entry via SOCE in the pancreatic β-cell model (supplementary material Fig. S2B), emphasizing the general validity of the specific inhibitory effect of NAGly on SOCE described herein. Notably, the latter experiments were performed in the presence of the K^+ channel opener diazoxide in order to prevent any Ca^{2+} entry through voltage-dependent Ca^{2+} channels (Dyachok and Gylfe, 2001).

To further investigate whether NAGly specifically targets the STIM1–Orai1-mediated SOCE, NAGly was tested on cells overexpressing both STIM1 and Orai1 (Mercer et al., 2006). As shown in Fig. 2C, NAGly was highly effective in attenuating increased SOCE signals, which led us to hypothesize that NAGly might reduce SOCE signals by disturbing the STIM1–Orai1 machinery itself.

STIM1 oligomerization and clustering upon ER Ca^{2+} depletion is insensitive to NAGly

The activation of SOCE upon ER Ca^{2+} depletion involves complex molecular processes starting with the oligomerization of STIM1 proteins, which subsequently redistribute to large STIM1 clusters in the subplasmalemmal area (Wu et al., 2006; Liou et al., 2007; Luik et al., 2008). In order to test whether or not NAGly affects STIM1 oligomerization, this process was monitored by measuring Förster resonance energy transfer (FRET) between the cyan fluorescent protein (CFP) and the yellow fluorescent protein (YFP) fused to the luminal N-terminus of STIM1 (Malli et al., 2008; Muik et al., 2008). Fast and strong ER Ca^{2+} depletion was achieved by cell treatment with Tg/His in the absence of extracellular Ca^{2+}, which triggered a rapid increase of the FRET signal between CFP–STIM1 and YFP–STIM1. This elevated FRET signal remained stable in the absence of extracellular Ca^{2+}, indicating a robust and constant oligomerization of STIM1 (Fig. 3A). Addition of NAGly did not reduce STIM1 oligomerization, indicating that this essential step in the activation of SOCE is insensitive to NAGly (Fig. 3A). Identical results were obtained in experiments where the fluorophores were at the C-terminus of STIM1, thus, being localized in the cytosol (supplementary material Fig. S3). In line with this finding, the stability of STIM1 clusters in ER Ca^{2+} depleted cells was not affected by NAGly either (Fig. 3B,C). We have previously reported that an increase in $[Ca^{2+}]_{cyto}$ reduces the amount of subplasmalemmal STIM1 clusters even in the virtual absence of ER Ca^{2+} refilling and despite almost unchanged oligomerization of STIM1 (Malli et al., 2008). The effect of $[Ca^{2+}]_{cyto}$ to destabilize STIM1 clusters was slightly delayed in the presence of NAGly, (Fig. 3C, left panel) that might reflect the reduced Ca^{2+} entry. However, the potency of $[Ca^{2+}]_{cyto}$ to reduce the appearance of subplasmalemmal STIM1 clusters remained unchanged (Fig. 3C, right panel).

NAGly did not affect the colocalization of STIM1 and Orai1, but strongly diminished the STIM1–Orai1 interaction in ER Ca^{2+}-depleted cells

Since NAGly was ineffective in impairing STIM1 oligomerization and clustering, we further focused on the interaction between STIM1 and Orai1 as a possible molecular target of NAGly. It was suggested that subplasmalemmal STIM1 clusters function as traps for Orai1 proteins (Xu et al., 2006), whereupon an intermolecular switching mechanism within the cytosolic domain of STIM1 allows electrostatic interaction with

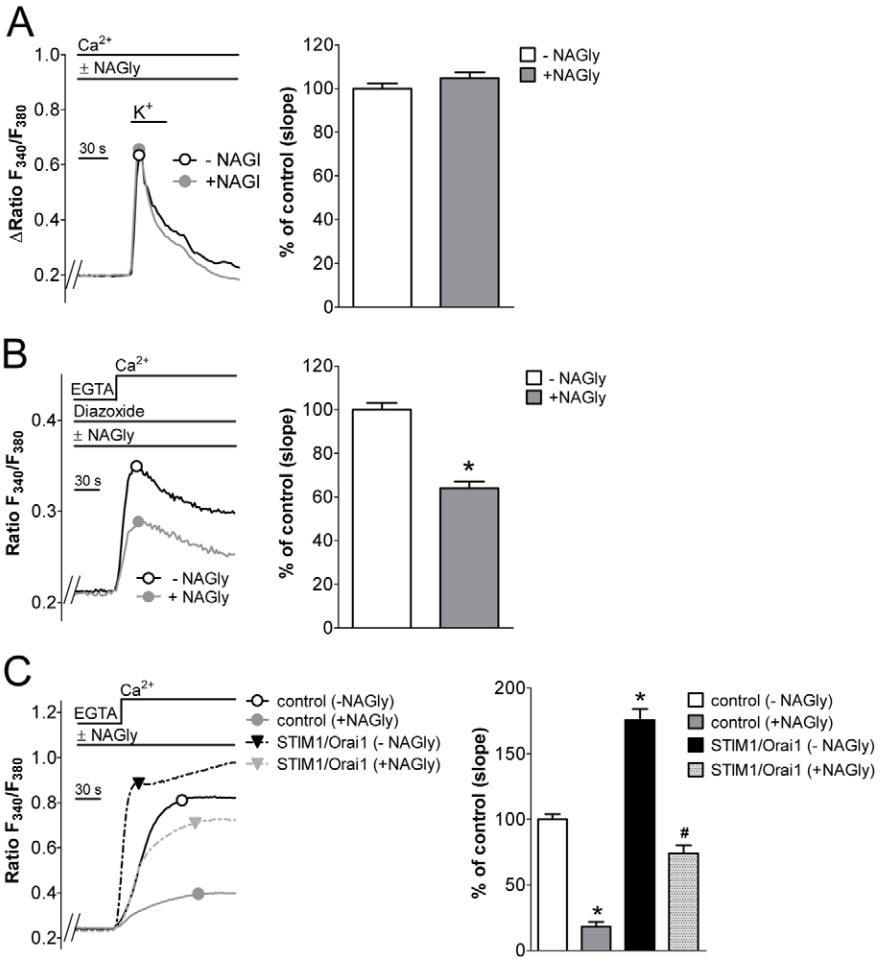

Fig. 2. NAGly specifically reduces SOCE in INS-1 and attenuates enhanced SOCE in endothelial cells overexpressing STIM1 and Orai1. (**A**) Left panel: voltage-dependent Ca^{2+} entry in Fura-2/AM-loaded INS-1 832/13 cells that were stimulated with 30 mM K^+ in the presence of 2 mM Ca^{2+} and 20 mM glucose without NAGly (black, $n=137/6$) or with 10 µM NAGly (grey, $n=131/6$). Right panel: bars represent slopes of Ca^{2+} increase as a percentage of control (−NAGly) calculated from the curves shown in the left panel. (**B**) Left panel: in the presence of 400 µM diazoxide and 20 mM glucose ER Ca^{2+} was depleted with 1 µM Tg. After 10 minutes, 2 mM Ca^{2+} was added in the absence (black, $n=137/6$) or presence of 10 µM NAGly (grey, $n=131/6$). Right panel: bars represent slopes of Ca^{2+} increase as a percentage of control (−NAGly) calculated from the curves shown in the left panel. *$P<0.001$ versus −NAGly. (**C**) Left panel: average curves of Fura-2/AM-loaded EA.hy926 cells in response to Ca^{2+} addition after ER Ca^{2+} depletion (using 1 µM Tg and 100 µM His) under control conditions without NAGly (black continuous line, $n=30/6$) with 10 µM NAGly (grey continuous line, $n=39/6$) and in cells coexpressing YFP–STIM1 and CFP–Orai1 in the absence (black dashed line, $n=38/8$) or presence of 10 µM NAGly (grey dashed line, $n=39/8$). Right panel: respective statistical analysis of data displayed in left panel. Mean slope of $[Ca^{2+}]_{cyto}$ increase is displayed as a percentage of untreated control cells expressing the cytosolic FP Venus. Slopes were calculated using linear regression between the initial onsets until the individual plateau phases were reached *$P<0.0001$ versus control (−NAGly). #$P<0.0001$ versus STIM1–Orai1 (−NAGly).

the C-terminal coiled-coil segment of Orai1 (Korzeniowski et al., 2010). Consistent with this intricate mechanism, the colocalization between YFP–STIM1 and CFP–Orai1 increased approximately twofold in response to ER Ca^{2+} depletion (Fig. 4A,C) as visualized by array confocal fluorescence microscopy setting the focal plane through the middle of individual cells. The addition of NAGly after ER Ca^{2+} depletion did not affect the increased colocalization between YFP–STIM1 and CFP–Orai1 in endothelial cells (Fig. 4B,C). Notably, these results were confirmed by confocal images across the surface of endothelial cells where a huge number of subplasmalemmal STIM1 clusters were detectable (supplementary material Fig. S4A,B).

Since colocalization experiments are not entirely conclusive on protein–protein interaction, a more sophisticated and detailed approach to study the interaction between STIM1 and Orai1 based on FRET was performed. In endothelial cells coexpressing Orai1–YFP and STIM1–CFP ER Ca^{2+} depletion decreased the donor CFP emission and increased the acceptor YFP emission simultaneously, resulting in a remarkable and long lasting increase in the FRET ratio (Fig. 4D), pointing to a stable interaction between the fusion proteins. Exposure to NAGly, however, led to a prompt reduction of the FRET signal due to a decrease in acceptor accompanied by an increase in donor emission intensities (Fig. 4D), indicating that the endocannabinoid diminished the molecular interaction between STIM1 and Orai1. In order to verify that NAGly indeed uncouples STIM1 and Orai1, we further examined their interaction by exchanging the donor and acceptor fluorescent proteins, respectively (i.e. measuring the FRET between STIM1–YFP and CFP–Orai1 (Fig. 4E; supplementary material Fig. S4C). In this setup, the basal ratio values ($F_{535[FRET]}/F480_{[DONOR]}$) were significantly lower, probably reflecting a different intracellular distribution of the two proteins. Nevertheless, ER Ca^{2+} depletion also evoked an increase in the STIM1–YFP/CFP–Orai1 FRET ratio, while NAGly treatment clearly decreased it (Fig. 4E; supplementary material Fig. S4C). These data demonstrate that NAGly efficiently diminishes STIM1–Orai1 FRET signals regardless of whether the FRET acceptor was fused to Orai1 or STIM1, thus, affirming that this endocannabinoid prevents STIM1–Orai1 interaction. Upon removal of NAGly the FRET signal between STIM1–CFP and Orai1–YFP recovered (Fig. 4F), which correlated with the reconstitution of Ca^{2+} entry via the SOCE pathway (Fig. 1C), thus, indicating that the inhibitory effect of NAGly on SOCE is a consequence of the diminished STIM1–Orai1 interaction. The inhibitory effect of NAGly on the interaction between STIM1 and Orai1 seemed to be specific, particularly in view of the finding that NAGly did not impact on STIM1 oligomerization (Fig. 3A; supplementary material Fig. S3). Moreover, in the respective control

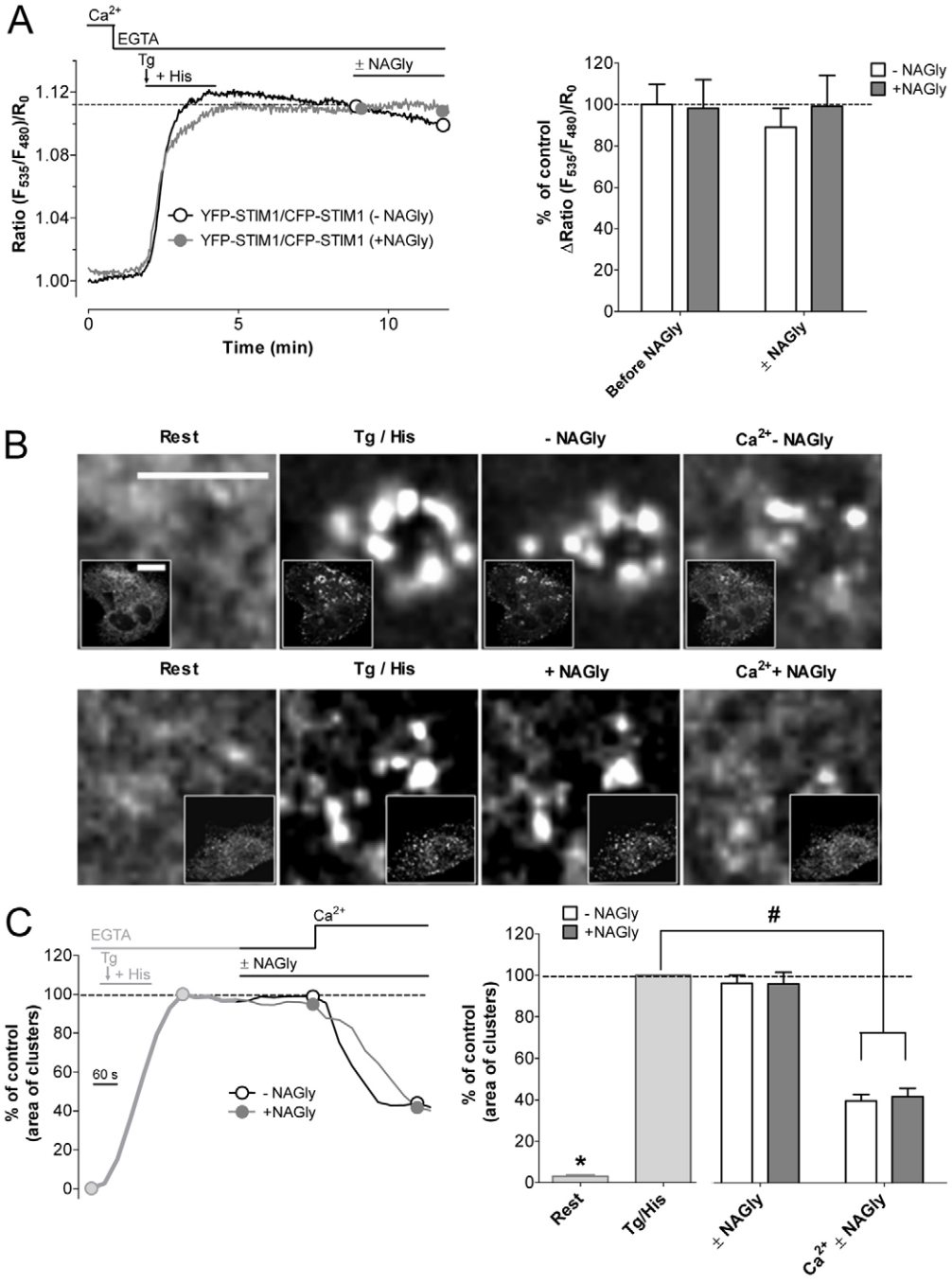

Fig. 3. NAGly does not affect STIM1 oligomerization or STIM1 clustering. (**A**) Left panel: dynamics of STIM1 oligomerization measured by FRET in EA.hy926 cells overexpressing YFP–STIM1 and CFP–STIM1. Oligomerization was triggered by 1 μM Tg and 100 μM His in the absence of extracellular Ca^{2+} and cells were subsequently treated with 10 μM NAGly (+NAGly, grey, $n=14/7$), while control cells (−NAGly, black, $n=16/7$) received no treatment. Right panel: bars represent the Δratio $(F_{535}/F_{480})/R_0$ from experiments presented in the left panel. FRET signals of control experiments before the addition of NAGly were defined as 100%. (**B**) Representative confocal images of subplasmalemmal STIM clusters with enlarged views (insets) in control (upper panel) and in NAGly-treated (lower panel) cells coexpressing YFP–STIM1 and CFP–Orai1 under resting condition (Rest), following 1 μM Tg and 100 μM His stimulation in the absence of Ca^{2+} (Tg/His), after ethanol (−NAGly) or 10 μM NAGly treatment (+NAGly) and subsequent 2 mM Ca^{2+} addition (Ca^{2+}). Scale bars: 10 μm. (**C**) Left panel: representative tracings of individual STIM1-cluster formation over time upon ER Ca^{2+} depletion and Ca^{2+} addition. Areas of clusters were normalized to respective individual maximal cluster areas (defined as 100%). Right panel: statistical analysis of STIM1-cluster areas under resting condition (Rest), after maximal store depletion (Tg/His), after ethanol (−NAGly) or NAGly treatment (+NAGly) and after Ca^{2+} addition (Ca^{2+}), as indicated. Bars represent mean STIM1-cluster areas of 10–15 clusters per cell in three independent experiments for both conditions. $^{*}P<0.0001$ versus cells treated with Tg/His in the absence of NAGly, $^{\#}P<0.0001$ versus Tg/His.

experiment NAGly did not affect the fluorescence ratio of Orai1–YFP and CFP–STIM1, which failed to show any increased FRET signal because of the different compartmentalization of the fluorophores (Fig. 4G). These findings indicate that the inhibitory effect of NAGly on the FRET signals between STIM1–CFP and Orai1–YFP or CFP–Orai1 and STIM1–YFP were indeed significant and not caused by an unspecific interference of NAGly with the fluorophores.

The putative involvement of mitochondria in the inhibitory action of NAGly on the STIM1–Orai1 interaction was tested using a mixture of antimycin A and oligomycin. This combination of mitochondrial toxins, which induces a strong and immediate depolarization of mitochondria, did not affect the STIM1–Orai1 interaction (supplementary material Fig. S4D). The subsequent addition of NAGly clearly reduced FRET signals between STIM1-CFP and Orai1–YFP in the presence of the mitochondrial toxins, supporting our assumption that the inhibitory effect of NAGly on SOCE is mainly independent of its effect on mitochondria.

In summary, our data provided herein unveiled a so far unknown inhibitory effect of the endocannabinoid NAGly on the signaling between STIM1 and Orai1. It is tempting to speculate that NAGly directly targets the STIM1–Orai1-containing SOCE machinery possibly by mimicking the negatively charged

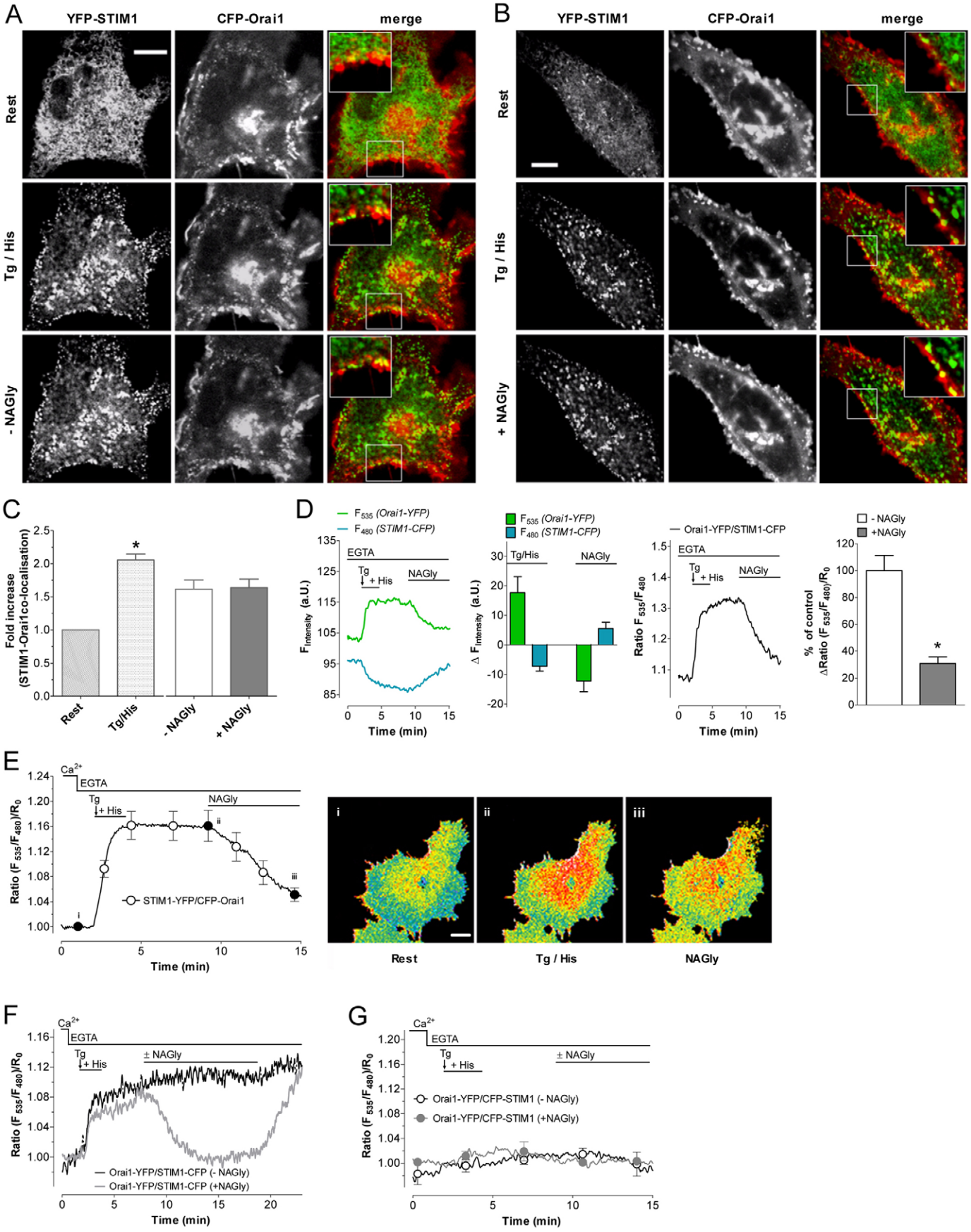

Fig. 4. See next page for legend.

C-terminal coiled-coil segment of Orai1, which might decouple the positively charged cytosolic domain of STIM1 from Orai1 (Korzeniowski et al., 2010). Alternatively, NAGly might accomplish SOCE inhibition via its binding to certain receptors (Kohno et al., 2006), thereby activating a downstream signaling pathway which subsequently affects the interaction between STIM1 and Orai1. Notably, mRNA levels of both GPR18 and GPR55, two putative receptors of NAGly, were detected in the endothelial cell line used (supplementary material Fig. S5). Further experiments are necessary to clarify the exact molecular mechanism by which NAGly affects the SOCE machinery. However, our experiments revealed that NAGly, but not AEA, is highly effective in inhibiting SOCE specifically in different cell types by impairing the interaction of STIM1 with Orai1, a phenomenon that might serve as an explanation for its distinct physiological effects.

Fig. 4. NAGly does not affect the colocalization between STIM1 and Orai1 but diminishes STIM1–Orai1 interaction. (**A**) Confocal images of EA.hy926 cells coexpressing YFP–STIM1 (left images) and CFP–Orai1 (middle images) and respective merges (right images) with enlarged views of the ER–PM junctions (insets) under resting conditions (upper panel), upon ER Ca^{2+} depletion with 1 μM Tg and 100 μM His after 4 minutes (middle panel) and 12 minutes without NAGly (lower panel). Scale bars: 10 μm. (**B**) Confocal images of cells treated as for A, except that the lower images show a representative cell treated with 10 μM NAGly in the presence of Tg and His. Scale bars: 10 μm. (**C**) Statistical analysis of YFP–STIM1 and CFP–Orai1 colocalization under conditions as in A (−NAGly, n=10/10) and B (+NAGly, n=11/11). STIM1–Orai1colocalization in individual cells upon stimulation was normalized to the respective colocalization under resting conditions. *P<0.0001 versus Rest. (**D**) Dynamic FRET measurements between Orai1–YFP and STIM1–CFP corresponding to STIM1–Orai1 interaction in EA.hy926 cells. Interaction was triggered with 1 μM Tg and 100 μM His in the absence of extracellular Ca^{2+} and cells were subsequently exposed to 10 μM NAGly, Left panel: representative tracings of individual FRET YFP (green) and CFP (cyan) emission signals over time that were corrected for photobleaching. Left middle panel: statistical evaluation of intensity changes following Tg/His (left bars; n=6/6) and NAGly treatment (right bars; n=6/6). Right middle panel: representative tracing of changes in FRET ratio calculated from intensity values shown in left panel. Right panel: statistical evaluation of the inhibitory effect of NAGly on STIM1–Orai1 interaction. The grey bar represents an average of normalized ΔFRET ratios 3 minutes after addition of 10 μM NAGly (+NAGly; n=14/9), and the white bars shows the average of the respective ΔFRET ratios of untreated cells (−NAGly, n=15/8). The maximal FRET signal at the time point before NAGly addition was defined as 100%. *P<0.0001 versus −NAGly. (**E**) Dynamic FRET measurements between STIM1–YFP and CFP–Orai1 in the experimental protocol described above. Left panel: dynamic changes of normalized average FRET ratios over time (n=7/5). Right panel: representative pseudocoloured FRET images of YFP/CFP ratio of cells under basal conditions (i), following Tg/His stimulation (ii), and after NAGly treatment (iii). Increased FRET signals appear as red pixels. Scale bar: 10 μm. (**F**) Representative tracings demonstrating the reversible effect of NAGly on STIM1–Orai1interaction in Orai1-YFP/STIM1-CFP-transfected cells. (**G**) Dynamic measurements of fluorescence signals in EA.hy926 cells coexpressing Orai1–YFP and CFP–STIM1. Notably, as the CFP was fused to the N-terminus of STIM1 facing the lumen of the ER, FRET between CFP–STIM1 and Orai1–YFP was absent because of the different compartmentalization of the respective fluorophores. Cells were stimulated with Tg/His in the absence of extracellular Ca^{2+} and subsequently exposed to 10 μM NAGly (+NAGly, grey, n=8/6) while control cells (−NAGly, black, n=7/5) received no treatment.

Materials and Methods

Chemicals and buffer solutions

Cell culture materials were obtained from PAA laboratories (Pasching, Austria). *N*-Arachidonoylglycin was from Tocris Bioscience (Bristol, UK); anandamide and thapsigargin were purchased from Abcam® (London, UK); histamine, diazoxide, 1,4-dihydroxy-2,5-di-tert-butylbenzene (BHQ) and EGTA were from Sigma (Vienna, Austria).

Prior to experiments, cells were washed and maintained for 20 minutes in a HEPES-buffered solution composed of (in mM): 138 NaCl, 5 KCl, 2 $CaCl_2$, 1 $MgCl_2$, 1 HEPES, 2.6 $NaHCO_3$, 0.44 KH_2PO_4, 0.34 Na_2HPO_4, 10 D-glucose, 0.1% vitamins, 0.2% essential amino acids and 1% penicillin/streptomycin; pH adjusted to 7.4 with NaOH. During the experiments cells were continuously perfused with a Ca^{2+}-containing buffer, which consisted of (in mM) 145 NaCl, 5 KCl, 2 $CaCl_2$, 1 $MgCl_2$, 10 D-glucose and 10 HEPES; pH adjusted to 7.4 with NaOH. In experiments where a Ca^{2+}-free solution was applied, the $CaCl_2$ was replaced with 1 mM EGTA. INS cells were stimulated with a buffer containing (in mM): 113 NaCl, 30 KCl, 2 $CaCl_2$, 1 $MgCl_2$, 20 D-glucose and 10 HEPES; pH adjusted to 7.4 with KOH.

Cell culture and transfection

The EA.hy926 (human umbilical vein-derived endothelial) cell line, INS-1 832/13 pancreatic β-cells, and RBL-2H3 (rat basophil leukaemia) cells were used for this study and cultured as described previously (Alam et al., 2012; Malli et al., 2007; Schindl et al., 2002).

Cells were transfected with 1.5 μg of plasmid DNA (per 30 mm well) and 2.5 μg/well TransFast™ transfection reagent (Promega, Madison, USA) in 1 ml of serum and antibiotic-free transfection medium 24 hours prior to experiments.

Constructs

For the overexpression of YFP- or CFP-tagged STIM1 and Orai1 proteins, respectively, the following N- or C-terminally tagged constructs were used: CFP-Orai1, YFP-STIM1, CFP-STIM1 as well as Orai1-YFP, STIM1-YFP, and STIM1-CFP (Frischauf et al., 2009; Muik et al., 2008; Malli et al., 2008).

Ca^{2+} and FRET imaging using fluorescence microscopy

For cytosolic Ca^{2+} measurements single-cell Ca^{2+}-imaging was performed as described previously (Graier et al., 1998; Malli et al., 2007). Briefly, cells were loaded with 2 μM Fura-2/AM (TEFLabs, Austin, TX, USA) for 45 minutes. Fura-2/AM-loaded cells were imaged using a fluorescence microscope described previously (Malli et al., 2007). For CFP/YFP-based FRET experiments cells were excited at 440 nm (440AF21; Omega Optical, Brattleboro, VT) and emission was gathered at 480 and 535 nm using an optical beam splitter (Dual View Micro-Imager™; Optical Insights, Visitron Systems) equipped with emission filters (480AF30, 535AF26; Omega Optical, Brattleboro, VT). Regions of interest covered whole individual cells. Results of FRET measurements are shown as the ratio of $(F_{535}/F_{480})/R_0$ to correct for photobleaching and/or photochromism, as described recently (Waldeck-Weiermair et al., 2012; Malli et al., 2008).

Confocal analysis

High resolution imaging of YFP–STIM1 and CFP–Orai1 was performed with an array confocal laser scanning microscope (ACLSM), built on an inverse, fully automatic microscope (Axio Observer.Z1 from Zeiss, Göttingen, Germany) using a 100×/1.45 NA oil immersion objective (Plan-Fluor, Zeiss), and 405 nm (120 mW diode laser, Visitron Systems) and 488 nm (50 mW, VSLaserModul, Visitron Systems) laser light for exciting CFP and YFP, respectively. Emission was acquired with a CCD camera (CoolSNAP-HQ, Photometrics, Tucson, AZ, USA) using the emission filters ET480/40m for CFP and ET535/30m for YFP (Chroma Technology Corporation, VT, USA). All devices were controlled by VisiView Premier acquisition software (Visitron Systems). Image analysis was performed with MetaMorph 7.7.0.0 (Visitron Systems) using the integrated morphometric analysis tool and the colocalization application.

Mitochondrial membrane potential

EA.hy926 cells were loaded with 150 nM tetramethylrhodamine methyl ester (TMRM) for 30 min at room temperature. All subsequent experiments were performed in quench mode with solutions as indicated in Chemicals and buffer solutions but containing 150 nM TMRM. TMRM fluorescence intensities of single cells were measured over non-mitochondrial (nuclear) regions using a 40× oil immersion objective on a Zeiss AxioVert inverted microscope (Zeiss, Austria) equipped with a polychromator illumination system (Visitron Systems, Germany) and a CCD camera (Photometrics, AZ, USA). TMRM was excited at 548 nm and emission was detected at 570 nm.

Mitochondrial pH

EA.hy926 cells stably expressing mitochondrial targeted pericam were used to measure the mitochondrial pH. Cells were illuminated at 480 nm and emission was

collected at 535 nm using the same imaging system described above. At the end of each individual experiment 2 μM FCCP was used to induce maximal mitochondrial acidification.

Real-time PCR

RNA was isolated from Ea.hy926 cells using a Total RNA isolation kit (PEQLAB Biotechnologie GmbH, Erlangen, Germany) and it was reverse transcribed using a High Capacity cDNA Reverse Transcription Kit (Applied Biosystems, USA). The analysis of the expression of the target genes was performed by conventional polymerase chain reaction (PCR) using GoTaq Green master mix (Promega, Madison, WI, USA) and real-time PCR using QuantiFast SYBR Green RT-PCR kit (Qiagen, Hilden, Germany) on LightCycler 480 (Roche Diagnostics, Vienna, Austria). RNA polymerase II (RPOL2) was used as a housekeeping control. Primers for RPOL2, GPR18 and GPR55 were obtained from Invitrogen (Vienna, Austria) and their sequences (5′–3′) are as follows: RPOL2 for: CATTGACTTG-CGTTTCCACC, RPOL2 rev: ACATTTTGTGCAGAGTTGGC; GPR18 for: CCACCTTCCTCATGAACCTC, GPR18 rev: GACCGTAGACTACCAGATCG; GPR55 for: TTGACGGTGTCAACGAGCTG, GPR55 rev: TAAGGAAGGTG-CTGAAGCCA.

Statistics

Data shown are means ± s.e.m., and *n* indicates the number of cells/independent experiments. Statistical analyses were performed with paired and unpaired Student's *t*-tests, and $P<0.05$ was considered to be significant.

Acknowledgements

We thank Therese Macher and Dr Rene Rost for their excellent technical assistance, Dr C. J. S. Edgell (University of North Carolina, Chapel Hill, NC, USA) for the EA.hy926 cells and Dr C. B. Newgard (Duke University, Durham NC, USA) for the INS-1 cells. Moreover we thank Prof. Christoph Romanin (University of Linz, Austria) for sending us the FP-tagged STIM1 and Orai1 constructs. We are grateful to Dr Maud Frieden (University of Geneva), Prof. Klaus Groschner, Mag. Karin Osibow, and Dr Michael Poteser (Medical University of Graz, Austria) for their critical comments.

Funding

This work was supported by the Austrian Science Funds (FWF) [grant numbers P21857-B18 and P22553-B18 to W.F.G. and R.M., respectively]. A.T.D. is funded by the FWF within the PhD program Neuroscience at the Medical University of Graz. M.R.A. and E.S. are funded by the FWF within the PhD program MolMed of the Medical University of Graz. Deposited in PMC for immediate release.

Supplementary material available online at
http://jcs.biologists.org/lookup/suppl/doi:10.1242/jcs.118075/-/DC1

References

Alam, M. R., Groschner, L. N., Parichatikanond, W., Kuo, L., Bondarenko, A. I., Rost, R., Waldeck-Weiermair, M., Malli, R. and Graier, W. F. (2012). Mitochondrial Ca^{2+} uptake 1 (MICU1) and mitochondrial Ca^{2+} uniporter (MCU) contribute to metabolism-secretion coupling in clonal pancreatic β-cells. *J. Biol. Chem.* **287**, 34445-34454.

Barbara, G., Alloui, A., Nargeot, J., Lory, P., Eschalier, A., Bourinet, E. and Chemin, J. (2009). T-type calcium channel inhibition underlies the analgesic effects of the endogenous lipoamino acids. *J. Neurosci.* **29**, 13106-13114.

Bondarenko, A. I., Malli, R. and Graier, W. F. (2011a). The GPR55 agonist lysophosphatidylinositol directly activates intermediate-conductance Ca^{2+}-activated K+ channels. *Pflugers Arch.* **462**, 245-255.

Bondarenko, A. I., Malli, R. and Graier, W. F. (2011b). The GPR55 agonist lysophosphatidylinositol acts as an intracellular messenger and bidirectionally modulates Ca^{2+} -activated large-conductance K+ channels in endothelial cells. *Pflugers Arch.* **461**, 177-189.

Bradshaw, H. B., Rimmerman, N., Hu, S. S. J., Benton, V. M., Stuart, J. M., Masuda, K., Cravatt, B. F., O'Dell, D. K. and Walker, J. M. (2009). The endocannabinoid anandamide is a precursor for the signaling lipid N-arachidonoyl glycine by two distinct pathways. *BMC Biochem.* **10**, 14.

Brunner, F., Stessel, H., Simecek, S., Graier, W. and Kukovetz, W. R. (1994). Effect of intracellular Ca^{2+} concentration on endothelin-1 secretion. *FEBS Lett.* **350**, 33-36.

Burstein, S. H., McQuain, C. A., Ross, A. H., Salmonsen, R. A. and Zurier, R. E. (2011). Resolution of inflammation by N-arachidonoylglycine. *J. Cell. Biochem.* **112**, 3227-3233.

Dyachok, O. and Gylfe, E. (2001). Store-operated influx of Ca^{2+} in pancreatic beta-cells exhibits graded dependence on the filling of the endoplasmic reticulum. *J. Cell Sci.* **114**, 2179-2186.

Feske, S., Gwack, Y., Prakriya, M., Srikanth, S., Puppel, S. H., Tanasa, B., Hogan, P. G., Lewis, R. S., Daly, M. and Rao, A. (2006). A mutation in Orai1 causes immune deficiency by abrogating CRAC channel function. *Nature* **441**, 179-185.

Frischauf, I., Muik, M., Derler, I., Bergsmann, J., Fahrner, M., Schindl, R., Groschner, K. and Romanin, C. (2009). Molecular determinants of the coupling between STIM1 and Orai channels: differential activation of Orai1-3 channels by a STIM1 coiled-coil mutant. *J. Biol. Chem.* **284**, 21696-21706.

Graier, W. F., Sturek, M. and Kukovetz, W. (1994). Ca^{2+} regulation and endothelial vascular function. *Endothelium* **1**, 223-236.

Graier, W. F., Paltauf-Doburzynska, J., Hill, B. J., Fleischhacker, E., Hoebel, B. G., Kostner, G. M. and Sturek, M. (1998). Submaximal stimulation of porcine endothelial cells causes focal Ca^{2+} elevation beneath the cell membrane. *J. Physiol.* **506**, 109-125.

Graier, W. F., Frieden, M. and Malli, R. (2007). Mitochondria and Ca^{2+} signaling: old guests, new functions. *Pflugers Arch.* **455**, 375-396.

Huang, S. M., Bisogno, T., Petros, T. J., Chang, S. Y., Zavitsanos, P. A., Zipkin, R. E., Sivakumar, R., Coop, A., Maeda, D. Y., De Petrocellis, L. et al. (2001). Identification of a new class of molecules, the arachidonyl amino acids, and characterization of one member that inhibits pain. *J. Biol. Chem.* **276**, 42639-42644.

Izzo, A. A., Fezza, F., Capasso, R., Bisogno, T., Pinto, L., Iuvone, T., Esposito, G., Mascolo, N., Di Marzo, V. and Capasso, F. (2001). Cannabinoid CB1-receptor mediated regulation of gastrointestinal motility in mice in a model of intestinal inflammation. *Br. J. Pharmacol.* **134**, 563-570.

Jousset, H., Malli, R., Girardin, N., Graier, W. F., Demaurex, N. and Frieden, M. (2008). Evidence for a receptor-activated Ca^{2+} entry pathway independent from Ca2) store depletion in endothelial cells. *Cell Calcium* **43**, 83-94.

Kohno, M., Hasegawa, H., Inoue, A., Muraoka, M., Miyazaki, T., Oka, K. and Yasukawa, M. (2006). Identification of N-arachidonylglycine as the endogenous ligand for orphan G-protein-coupled receptor GPR18. *Biochem. Biophys. Res. Commun.* **347**, 827-832.

Korzeniowski, M. K., Manjarrés, I. M., Varnai, P. and Balla, T. (2010). Activation of STIM1-Orai1 involves an intramolecular switching mechanism. *Sci. Signal.* **3**, ra82.

Kunos, G., Bátkai, S., Offertáler, L., Mo, F., Liu, J., Karcher, J. and Harvey-White, J. (2002). The quest for a vascular endothelial cannabinoid receptor. *Chem. Phys. Lipids* **121**, 45-56.

Liou, J., Kim, M. L., Heo, W. D., Jones, J. T., Myers, J. W., Ferrell, J. E., Jr and Meyer, T. (2005). STIM is a Ca^{2+} sensor essential for Ca^{2+}-store-depletion-triggered Ca^{2+} influx. *Curr. Biol.* **15**, 1235-1241.

Liou, J., Fivaz, M., Inoue, T. and Meyer, T. (2007). Live-cell imaging reveals sequential oligomerization and local plasma membrane targeting of stromal interaction molecule 1 after Ca^{2+} store depletion. *Proc. Natl. Acad. Sci. USA* **104**, 9301-9306.

Lückhoff, A., Pohl, U., Mülsch, A. and Busse, R. (1988). Differential role of extra- and intracellular calcium in the release of EDRF and prostacyclin from cultured endothelial cells. *Br. J. Pharmacol.* **95**, 189-196.

Luik, R. M., Wang, B., Prakriya, M., Wu, M. M. and Lewis, R. S. (2008). Oligomerization of STIM1 couples ER calcium depletion to CRAC channel activation. *Nature* **454**, 538-542.

Malli, R., Frieden, M., Osibow, K., Zoratti, C., Mayer, M., Demaurex, N. and Graier, W. F. (2003). Sustained Ca^{2+} transfer across mitochondria is essential for mitochondrial Ca^{2+} buffering, sore-operated Ca^{2+} entry, and Ca^{2+} store refilling. *J. Biol. Chem.* **278**, 44769-44779.

Malli, R., Frieden, M., Hunkova, M., Trenker, M. and Graier, W. F. (2007). Ca^{2+} refilling of the endoplasmic reticulum is largely preserved albeit reduced Ca^{2+} entry in endothelial cells. *Cell Calcium* **41**, 63-76.

Malli, R., Naghdi, S., Romanin, C. and Graier, W. F. (2008). Cytosolic Ca^{2+} prevents the subplasmalemmal clustering of STIM1: an intrinsic mechanism to avoid Ca^{2+} overload. *J. Cell Sci.* **121**, 3133-3139.

Mechoulam, R. (2002). Discovery of endocannabinoids and some random thoughts on their possible roles in neuroprotection and aggression. *Prostaglandins Leukot. Essent. Fatty Acids* **66**, 93-99.

Mercer, J. C., Dehaven, W. I., Smyth, J. T., Wedel, B., Boyles, R. R., Bird, G. S. and Putney, J. W., Jr (2006). Large store-operated calcium selective currents due to co-expression of Orai1 or Orai2 with the intracellular calcium sensor, Stim1. *J. Biol. Chem.* **281**, 24979-24990.

Muik, M., Frischauf, I., Derler, I., Fahrner, M., Bergsmann, J., Eder, P., Schindl, R., Hesch, C., Polzinger, B., Fritsch, R. et al. (2008). Dynamic coupling of the putative coiled-coil domain of ORAI1 with STIM1 mediates ORAI1 channel activation. *J. Biol. Chem.* **283**, 8014-8022.

Naghdi, S., Waldeck-Weiermair, M., Fertschai, I., Poteser, M., Graier, W. F. and Malli, R. (2010). Mitochondrial Ca^{2+} uptake and not mitochondrial motility is required for STIM1-Orai1-dependent store-operated Ca^{2+} entry. *J. Cell Sci.* **123**, 2553-2564.

Nitert, M. D., Nagorny, C. L. F., Wendt, A., Eliasson, L. and Mulder, H. (2008). CaV1.2 rather than CaV1.3 is coupled to glucose-stimulated insulin secretion in INS-1 832/13 cells. *J. Mol. Endocrinol.* **41**, 1-11.

Parekh, A. B. (2008). Mitochondrial regulation of store-operated CRAC channels. *Cell Calcium* **44**, 6-13.

Parekh, A. B. and Putney, J. W., Jr (2005). Store-operated calcium channels. *Physiol. Rev.* **85**, 757-810.

Park, C. Y., Hoover, P. J., Mullins, F. M., Bachhawat, P., Covington, E. D., Raunser, S., Walz, T., Garcia, K. C., Dolmetsch, R. E. and Lewis, R. S. (2009). STIM1 clusters and activates CRAC channels via direct binding of a cytosolic domain to Orai1. *Cell* **136**, 876-890.

Parmar, N. and Ho, W. S. V. (2010). N-arachidonoyl glycine, an endogenous lipid that acts as a vasorelaxant via nitric oxide and large conductance calcium-activated potassium channels. *Br. J. Pharmacol.* **160**, 594-603.

Pertwee, R. G. (2006). Cannabinoid pharmacology: the first 66 years. *Br. J. Pharmacol.* **147**, S163-S171.

Pozo-Guisado, E., Campbell, D. G., Deak, M., Alvarez-Barrientos, A., Morrice, N. A., Alvarez, I. S., Alessi, D. R. and Martín-Romero, F. J. (2010). Phosphorylation of STIM1 at ERK1/2 target sites modulates store-operated calcium entry. *J. Cell Sci.* **123**, 3084-3093.

Putney, J. W., Jr (1986). A model for receptor-regulated calcium entry. *Cell Calcium* **7**, 1-12.

Roos, J., DiGregorio, P. J., Yeromin, A. V., Ohlsen, K., Lioudyno, M., Zhang, S., Safrina, O., Kozak, J. A., Wagner, S. L., Cahalan, M. D. et al. (2005). STIM1, an essential and conserved component of store-operated Ca^{2+} channel function. *J. Cell Biol.* **169**, 435-445.

Schindl, R., Kahr, H., Graz, I., Groschner, K. and Romanin, C. (2002). Store depletion-activated CaT1 currents in rat basophilic leukemia mast cells are inhibited by 2-aminoethoxydiphenyl borate. Evidence for a regulatory component that controls activation of both CaT1 and CRAC (Ca^{2+} release-activated Ca^{2+} channel) channels. *J. Biol. Chem.* **277**, 26950-26958.

Schwindling, C., Quintana, A., Krause, E. and Hoth, M. (2010). Mitochondria positioning controls local calcium influx in T cells. *J. Immunol.* **184**, 184-190.

Shaw, P. J. and Feske, S. (2012). Physiological and pathophysiological functions of SOCE in the immune system. *Front. Biosci. (Elite Ed.)* **4**, 2253-2268.

Sheskin, T., Hanus, L., Slager, J., Vogel, Z. and Mechoulam, R. (1997). Structural requirements for binding of anandamide-type compounds to the brain cannabinoid receptor. *J. Med. Chem.* **40**, 659-667.

Tanasescu, R. and Constantinescu, C. S. (2010). Cannabinoids and the immune system: an overview. *Immunobiology* **215**, 588-597.

Vig, M., Peinelt, C., Beck, A., Koomoa, D. L., Rabah, D., Koblan-Huberson, M., Kraft, S., Turner, H., Fleig, A., Penner, R. et al. (2006). CRACM1 is a plasma membrane protein essential for store-operated Ca^{2+} entry. *Science* **312**, 1220-1223.

Waldeck-Weiermair, M., Zoratti, C., Osibow, K., Balenga, N., Goessnitzer, E., Waldhoer, M., Malli, R. and Graier, W. F. (2008). Integrin clustering enables anandamide-induced Ca^{2+} signaling in endothelial cells via GPR55 by protection against CB1-receptor-triggered repression. *J. Cell Sci.* **121**, 1704-1717.

Waldeck-Weiermair, M., Alam, M. R., Khan, M. J., Deak, A. T., Vishnu, N., Karsten, F., Imamura, H., Graier, W. F. and Malli, R. (2012). Spatiotemporal correlations between cytosolic and mitochondrial Ca^{2+} signals using a novel red-shifted mitochondrial targeted cameleon. *PLoS ONE* **7**, e45917.

Wiles, A. L., Pearlman, R. J., Rosvall, M., Aubrey, K. R. and Vandenberg, R. J. (2006). N-Arachidonyl-glycine inhibits the glycine transporter, GLYT2a. *J. Neurochem.* **99**, 781-786.

Wu, M. M., Buchanan, J., Luik, R. M. and Lewis, R. S. (2006). Ca^{2+} store depletion causes STIM1 to accumulate in ER regions closely associated with the plasma membrane. *J. Cell Biol.* **174**, 803-813.

Xu, P., Lu, J., Li, Z., Yu, X., Chen, L. and Xu, T. (2006). Aggregation of STIM1 underneath the plasma membrane induces clustering of Orai1. *Biochem. Biophys. Res. Commun.* **350**, 969-976.

Yuan, J. P., Zeng, W., Dorwart, M. R., Choi, Y. J., Worley, P. F. and Muallem, S. (2009). SOAR and the polybasic STIM1 domains gate and regulate Orai channels. *Nat. Cell Biol.* **11**, 337-343.

Zaccagnino, P., Saltarella, M., D'Oria, S., Corcelli, A., Saponetti, M. S. and Lorusso, M. (2009). N-arachidonylglycine causes ROS production and cytochrome c release in liver mitochondria. *Free Radic. Biol. Med.* **47**, 585-592.

Zygmunt, P. M., Petersson, J., Andersson, D. A., Chuang, H., Sørgård, M., Di Marzo, V., Julius, D. and Högestätt, E. D. (1999). Vanilloid receptors on sensory nerves mediate the vasodilator action of anandamide. *Nature* **400**, 452-457.